MODELING BRINE REFLUX USING THE PITZER ION-INTERACTION MODEL IN TOUGHREACT

Anwar Al-Helal[1], Fiona F. Whitaker[1], Nicolas Spycher[2], Yitian Xiao[3]

[1]Department of Earth Sciences, University of Bristol,
Bristol BS8 1RJ, England,
[2]Lawrence Berkeley National Laboratory,
Earth Sciences Division, Berkeley, CA 94720, USA
[3]ExxonMobil Exploration Company, PO Box 2189, Houston TX 77027, USA
An.Alhelal@bristol.ac.uk

ABSTRACT

Reflux of a penesaline (186‰) brine and resulting water-rock interactions were simulated using a modification of TOUGHREACT that incorporates the Pitzer ion-interaction theory. The brine is sourced from a 5 km wide brine pool in the interior of a 25 km wide platform and flows basinward through a 3 km thick sequence of grain-dominated packstone sediments. Ion interactions reduce dolomite supersaturation and anhydrite undersaturation predicted using the Pitzer approach compared with the Debye-Hückel approach, but increase calcite undersaturation. This increased undersaturation, combined with enhanced fluid flow above a shallower zone of anhydrite precipitation, results in more rapid dolomitization despite the lower initial dolomite saturation.

The penesaline brines reflux at up to 7 my^{-1}, three times the maximum flow rate in identical simulations involving a mesohaline (85‰) brine, in direct proportion to the difference in the density gradient. However, dolomitization is an order of magnitude faster for the penesaline brine, with replacement of all limestone to a depth of 43 m within 50 ky. Even after 1 My of penesaline-brine reflux, alteration is largely limited to sediments underlying the brine pool. In contrast, the penesaline brine forms a tabular dolomite body extending some 20 km to the platform margin. The upper 200 m of porous dolomite, lacking significant primary dolomite cements, overlies a thick (>700 m) zone where anhydrite cements plug up to 25% of the porosity. Penesaline brine reflux forms less anhydrite cement, due both to slower anhydrite precipitation (driven by slower upstream dolomitization), and to more .rapid anhydrite dissolution once dolomitization is complete.

INTRODUCTION

Dolomites are a common component of the carbonate rock record, and many were inferred to have formed by reflux of brines through carbonate platforms during early burial. Previous reactive transport modeling (RTM) simulations using TOUGHREACT have demonstrated the diagenetic potential of penesaline brine reflux, and the importance of coupled simulation of solute and heat flux (Al-Helal et al., 2012). We also evaluated sensitivity to the degree of evaporative concentration of the source seawater, via controls on both density-dependent fluid flow rate and chemical composition of reactive fluids. However, the standard version of TOUGHREACT uses the HKF model, based on the Debye-Hückel approach, limiting simulations, which is not reliable for high ionic strength brines.

This study uses a modification of TOUGHREACT that incorporates the Pitzer ion-interaction theory to simulate the reflux of penesaline brines, and compares this with mesohaline reflux, in a large-scale isolated carbonate platform over the timescale of up to one million years (1My). The code incorporates two alternative means of calculating the activity coefficient with respect to pre-estimating the ionic strength: the Helgeson-Kirkham-Flowers (HKF) model (Xu et al., 2004) and the Harvie-Møller-Weare (HMW) model (Zhang et al., 2006a,b).

The standard HKF model, based on the Debye-Hückel approach, is applicable only for dilute to moderately saline waters (<3 molal or 130 ‰) where NaCl is the dominant electrolyte. This approximates the upper range of salinity for mesahaline brines (35-140‰, Warren 1999). For higher ionic strength, solutions with many sepa-

rate ion pairs (secondary species), the Newton–Raphson method employed may converge slowly and to inaccurate results, or may fail to converge. However, when using the HMW model, which considers ion pairing directly through ion-interaction coefficients, simulations typically converge in fewer iterations and produce a more accurate representation of ionic activity. This tends to reduce the overestimation of ionic activity for high solutions with high total molality (Boyd, 1981; Table.1).

METHODS

Flow was simulated in a high-resolution 2D flow domain, using linear (Cartesian) coordinates. The flat-topped shelf measures 25 km from the margin to the interior, with a steep margin sloping down into a 2 km deep basin. The grid system comprises 2964 active blocks of non-uniformly specified node spacing, with reduction in cell width from 1250 m to 250 m and height from 100 m to 1 m (Figure 1). This could represent half of a symmetrical 50 km wide isolated carbonate platform, where brines are formed by evaporation of seawater, or a 25 km wide attached shelf, with no additional component of groundwater discharge from continental source to the right of the modeled domain except to the brine pool.

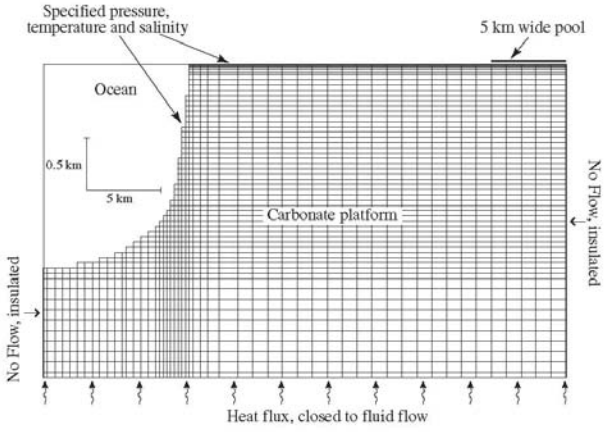

Figure 1. 2D RTM simulation grid and boundary conditions for the current study

Right and left boundaries are no-flow boundaries, while the lower boundary is closed to flow and solute transport but open to heat transport, with a specified heat flux of 60 mW/m^2, representative of a passive margin setting. The upper boundary is a fluid-pressure boundary, allowing the recharge or discharge of fluids at the platform top and slope. The platform top temperature is specified as 40°C and the ocean temperature declines exponentially with depth after Sanford et al. (1998).

The initial porosity declines exponentially with depth based on core data for the Cenozoic and Mesozoic Florida carbonates (Schmoker and Halley, 1982). Permeability was derived from porosity based on grain-size-dependent relations of Lucia (1995). Permeability anisotropy was specified as 10^3 (horizontal to vertical), after flow-based scaled-up simulations (Jones 2000). Diagenetic changes in permeability were calculated from changes in porosity using the Carman-Kozeny relation, ignoring changes in grain size, tortuosity, and specific surface area.

The initial temperature and pressure reflects advective heat transport by geothermal convection. The fluids surrounding the platform are seawater evolved to equilibrium with respect to calcite. The brine pool temperature was set as 40°C, and two alternative brine compositions were specified; a penesaline brine (186‰ or 5.3×seawater) and a mesohaline brine (85‰ or 2.5×seawater). The brine compositions were derived from published analyses of Ralph Sink and Ibis Pond respectively, from the Lake MacLeod evaporite basin (Logan, 1987; Table.1).

Simulations incorporated three solid phases (calcite, dolomite, and anhydrite), with initial mineralogy specified to be 99% calcite and 1% "seed" dolomite. Dolomite is assumed to react under kinetic constraints, using the rate equation of Arvidson and Mackenzie (1999). Calcite and anhydrite, which react much faster, are considered to react locally at equilibrium. Reactive surface area (RSA) was set as 10^3 cm^2/g, based on the average grain size of a grain-dominated packstone sediment (Lucia, 1995) and/or medium crystalline mud-dominated dolostone (Lucia, 2004). Mineral abundance is reported as percentage of total mineral volume.

RESULTS

Comparison of HKF and HMW models for penesaline brines.

A number of key indicators were used to compare calculations of the potential of penesaline brines (186‰) from the HKF and the HMW models:

(1) The number of iterations required to calculate the ionic activity: The HMW model calculates the ionic activity using only four Newton–Ralphson iterations, half the number required by the HKF model.

(2)The difference between the stoichiometric and the true ionic strength: As would be expected, the HMW model yields a true ionic strength that is essentially identical to the stoichiometric ionic strength, because this model does not take into account the formation of separate (secondary) aqueous species to account for ion pairing. In contrast, using the HKF model, which includes secondary species, the two estimates of ionic strength differ for all waters considered, and this difference becomes really substantial for the penesaline brine, with the true ionic strength being about 69% of the stoichiometric ionic strength (Table 1).

Table 1. Chemical composition of initial and boundary fluids for the major ions (mol L^{-1}) from Logan (1987), saturation indices (SI) and ionic strength calculated at 40°C and atmospheric P_{CO2} using the HFK model and the HMW model.

Component	Seawater	Mesohaline Brine (Ibis Pond)	Penesaline Brine (Ralph Sink)
Salinity‰	35	85	186
pH	8.22	7.70	7.10
Na^+	$4.85e^{-1}$	$1.26e^{0}$	$3.18e^{0}$
Mg^{2+}	$5.51e^{-2}$	$1.37e^{-1}$	$3.39e^{-1}$
Ca^{2+}	$1.07e^{-2}$	$2.44e^{-2}$	$2.22e^{-2}$
K^+	$1.06e^{-2}$	$2.56e^{-2}$	$6.56e^{-2}$
Cl^-	$5.66e^{-1}$	$1.46e^{0}$	$3.69e^{0}$
SO_4^{-2}	$2.93e^{-2}$	$7.78e^{-2}$	$1.37e^{-1}$
HCO_3^-	$2.41e^{-3}$	$1.54e^{-3}$	$1.83e^{-3}$
Mg/Ca	5.1	5.6	15.3
Calculated saturation index using the HKF model			
SI calcite	0.89	0.34	-0.45
SI dolomite	3.70	2.63	1.52
SI anhydrite	-0.86	-0.42	-0.53
Ionic Strength			
Stoichiometric	0.72	1.85	4.47
True	0.64	1.50	3.07
Calculated saturation index using the HMW method			
SI calcite	0.60	*	-0.85
SI dolomite	3.54	*	1.41
SI anhydrite	-1.00	*	-0.40
Ionic Strength			
Stoichiometric	0.72	*	4.47
True	0.72	*	4.47

* not computed for this case.

(3) The calculated saturation indices of diagenetic minerals of interest (calcite, dolomite, and anhydrite): Results displayed in Table 1 and Figure 2 show that the application of the HMW model predicts brines have a greater potential to dissolve calcite compared with the HKF model, and a reduced anhydrite undersaturation. In addition, the HMW model significantly overestimates the extent of dolomite supersaturation in the initial penesaline brine solution. The differences in saturation indices result in a difference in computed mineral abundances using the two models. The interplay between kinetically controlled dolomitization and geologically instantaneous dissolution or precipitation of calcite and anhydrite are apparent from the 2D simulations discussed later.

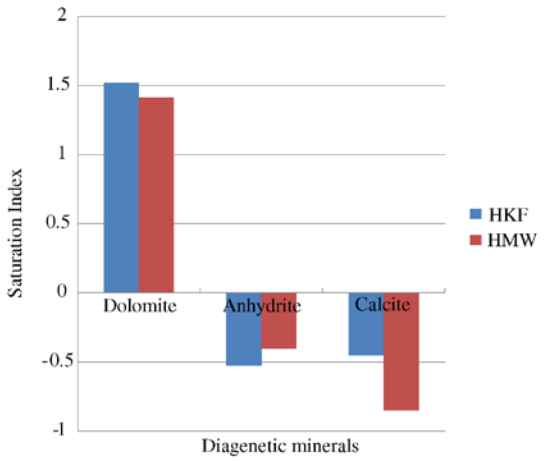

Figure 2. Comparison of the saturation indices for the penesaline brine (186‰) calculated using the HKF model (blue) and the HMW model (red).

(4) Predicted diagenesis: Calcite is dissolved and replaced by dolomite, consuming Mg^{2+} from solution and releasing Ca^{2+}, which then combines with the SO_4^{2-} to form calcium sulfate (modeled as anhydrite). The predicted change in abundance of dolomite and anhydrite, expressed in terms of total cross-sectional area after 1 My, indicates significant differences between the results of simulations using the MMW and HFK models (Figure 3).

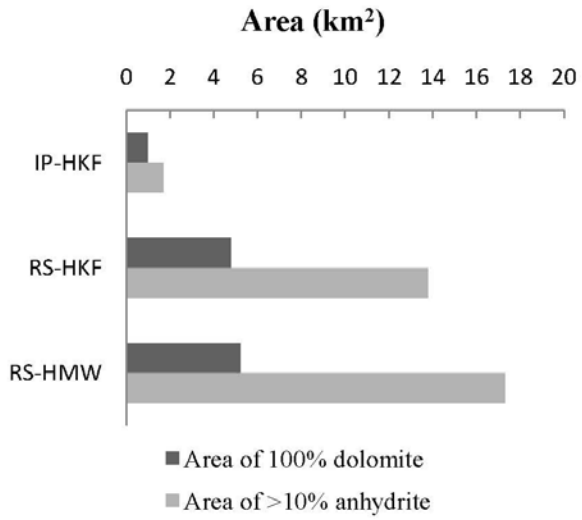

Figure 3. Comparison of reflux diagenesis in a grain-dominated packstone platform expressed in terms of total cross-sectional area exceeding 100% dolomite (dark bars) and 10% anhydrite (light bars) after 1 My for reflux of mesohaline (85‰) brines from Ibis Pond (IP) and penesaline (186 ‰) brines from Ralph Sink (RS) using both the HKF activity coefficient model and the HMW model.

Although the HMW predicts slightly lower dolomite supersaturation than the HKF model, the size of the completely dolomitized body was 9% greater due to more rapid calcite dissolution. The consequent enhanced release for Ca^{2+} into solution also promotes anhydrite precipitation downstream of the zone of dolomitization, with a 25% larger area of >10% anhydrite compared to the HKF model.

Subtle but important differences between predictions of the spatial distribution of diagenetic products using the two models after 1My are shown in Figure 4. For the HKF simulation, rapid fluid flux (>6 my^{-1}) occurs

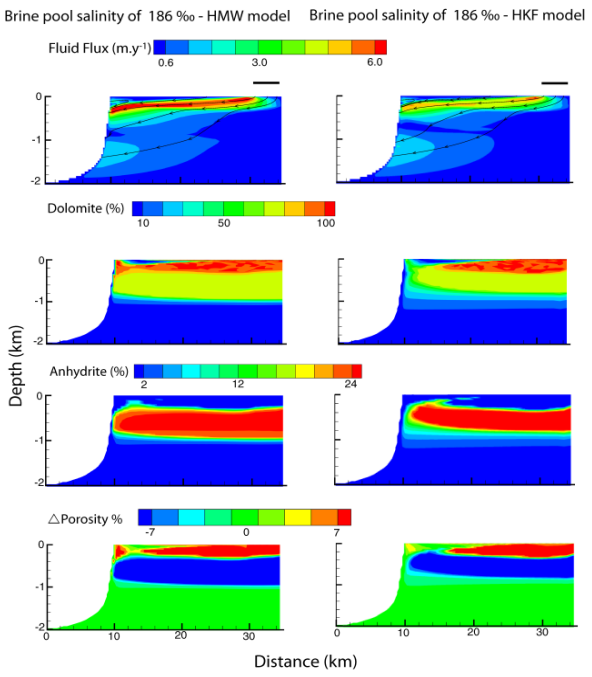

Figure 4. Simulations of fluid flux (with representative streamlines), dolomite and anhydrite abundance and change from initial porosity after 1 My of reflux of penesaline (186‰) brines using the HMW model (left) and the HKF activity coefficient model (right). The solid bar represents the 5 km wide brine pool.

only in a limited zone where the density gradient is highest, underlying the interface between the brine pool and the normal-salinity platform top fluids. In contrast these high rates of fluid flow extend across much of the platform in the HMW simulation, reflecting greater diagenetic enhancement of porosity and permeability at shallow depth, and pore-filling anhydrite precipitation beneath this.

Despite the higher calculated dolomite supersaturation for the penesaline brine, the HKF simulation underestimates the rate of dolomitization. This arises because the replacement reaction is driven in part by the dissolution of calcite, and the HKF model predicts a lesser degree of calcite undersaturation. Accordingly, the zone of complete dolomitization extends laterally some 20 km from the brine pool within 1 My in the HMW simulation, almost twice the extent of the dolomite body in the HKF simulation.

As a result of this, the HKF model underestimates both the depth of the anhydrite body and the area beneath the brine pool affected by dissolution of this secondary anhydrite. More rapid dolomitization increases the onset of downstream anhydrite precipitation. However, once dolomitization is complete, there is no release of Ca^{2+} to buffer the anhydrite undersaturation in the refluxing brines, and thus anhydrite dissolution occurs behind the dolomitization front. With more complete shallow dolomitization, the HMW simulation shows how the brine plume can supply Mg^{2+}-rich fluids to the platform margin, enhancing rates of dolomitization in the zone affected by geothermal convection, where waters are too cold to precipitate anhydrite.

Comparison between diagenesis driven by reflux of mesohaline and penesaline brines

Comparison was made between the penesaline 186‰ brines simulated using the HMW model and the mesohaline 85‰ brines simulated using the HKF model (Table 1) with stoichiometric ionic strengths of 4.47 and 1.85 respectively.

Table 1 highlights the distinct chemical differences between the two brines. The salinity of 186‰ brines is more than twice that of the 85‰ brines. The associated density difference between the penesaline brine and seawater is thus three times greater than that between the mesohaline brine and seawater.In parallel, the Mg/Ca molar ratio of the penesaline brine is almost 3 times higher than that of the mesohaline brine, which has a Mg/Ca only 1.1x that of seawater. The lower pH for the more concentrated brines is consistent with the general decrease in the pH with increasing chlorinity, described by Hanor (2001). In parallel, the measured bicarbonate alkalinity was higher in the high salinity brines.

At 1 My, the simulations showed that all diagenetic reactions were significantly more rapid in the penesaline-brine simulation and affect a larger area of the platform (Figure 5). There is a significant lateral extension of the dolomite body formed from the penesaline brine towards the margin, and dolomitization reaches ~1 km depth. In comparison, dolomitization by the

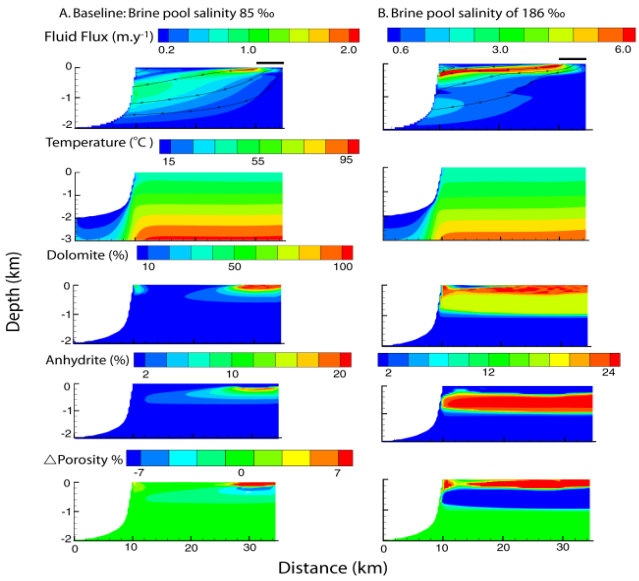

Figure 5. Simulations of fluid flux (with representative streamlines), temperature, dolomite and anhydrite abundance and change in initial porosity after 1 My of reflux of mesohaline (85‰) brines using the HKF model and penesaline (186‰) brines using the HMW model.

mesohaline brine remains focused beneath and immediately downstream of the brine pool.

The resulting enhanced formation of pore-occluding anhydrite in the penesaline reflux simulation provides a barrier preventing significant volumes of brines from circulating through the platform at depth. Rather, the majority of fluid flux, and diagenetic alteration, occurs in the upper 200 m, with lateral transfer and discharging into the ocean at the platform margin; beneath this, there is a broader zone of partial dolomitization.

The increased density contrast between the higher-salinity platform top brines and the ocean waters results in reflux at rates up to 2.5 times those in the mesohaline simulation (7 my^{-1} and 2.8 my^{-1} respectively). One consequence of the high fluid flux is advective cooling of the platform, by some 2.5°C at 500 m depth below the center of the brine pool, and twice this at 2.5 km depth (Figure 5).

The first very shallow occurrence of complete dolomitization is predicted to occur 135 ky earlier in the penesaline-brine simulation,

compared with 335 ky in the mesohaline simulation. The predicted spatial distribution of the penesaline reflux dolomite at 300 ky (plot not shown) is quite similar to that of the mesohaline reflux dolomite at 1 My (Figure 5).

One My of penesaline brine reflux produces a dolomite body with a cross-sectional area five times that of the mesohaline dolomite body, and the cross-sectional area of rock with anhydrite in excess of 10% is 10 times greater than the mesohaline simulation (Figure 3). The tabular-shaped body of penesaline-reflux dolomite extends laterally to join with the geothermal dolomite body. Reflux consequently feeds the geothermal convection cell with Mg^{2+}-rich fluids that increase the dolomitization rate in that area effected by geothermal convection, driving it to complete dolomitization within 1 My.

The mesohaline dolomites are largely restricted to a smaller area that extends <3 km laterally from the brine pool. The penesaline reflux results in a broad zone of complete dolomitization extending across much of the platform. Penesaline dolomites extend to a depth of ~900 m by 1 My, almost 5 times thicker than the dolomite zone predicted in the mesohaline simulation. Associated with the thicker body of dolomite, the underlying zone of partial dolomitization becomes thinner (a sharper "dolomite front").

Significant (≥20%) diagenetic anhydrite developed only after 1 My simulation of the mesohaline brines. Hence, the penesaline brine reflux results in a porosity reduction of 11%, more than double that of the mesohaline brines (5%). From this porosity reduction, the model predicts a permeability reduction of up to 3 darcy and 2 darcy respectively for the penesaline and mesohaline brine simulations .

In addition, the 1 My comparative simulations illustrate that, despite the marginally higher temperatures for mesohaline brine reflux, the predicted preservation of anhydrite cements behind the advancing dolomite front is some 5.6% lower than that of the penesaline case, reflecting the greater fraction of anhydrite formed during penesaline reflux. Figure (5) illustrates a much greater spatial overlap between the zone where porosity increases due to dolomitization and that of porosity reduction by anhydrite cementation. As a result, significant net porosity change is limited to a more limited zone at shallow depth beneath the mesasaline brine pool.

CONCLUSION

The main objective of this study was to highlight the importance of using an appropriate activity coefficient model for RTM simulations. Implementing the Pitzer approach via the HMW model in TOUGHREACT enabled us to simulate the diagenetic potential of penesaline brine reflux. The comparison between the simulated results of hyperaline brines of 186‰ salinity (4.47 ionic strength), using both the HKF and the HMW models, demonstrated that the results of the HKF model underestimates the diagenetic potential of refluxing brines compared to the HMW model, which is expected to be more accurate than the HKF model at high salinities.

Comparison of penesaline and mesohaline brine reflux quantified differences in the rate and distribution of dolomitization and anhydrite precipitation and dissolution. The diagenetic system proved to be critically sensitive to the salinity of the brines, via effects on both fluid flux and reaction rate.

ACKNOWLEDGMENTS

Funding for this study was provided by the public authority for applied education and training "Kuwait." ABA and FFW thank LBNL for supporting stimulating academic exchange visits between LBNL and Bristol.

REFERENCES

Al-Helal, A. B., Whitaker, F. F. and Xiao, Y. Reactive transport modeling of brine reflux: dolomitization, anhydrite precipitation, and porosity evolution. *J. Sediment. Res.,* 82(3), 196-215, 2012.

Arvidson, R. S., and Mackenzie, F. T., The dolomite problem - Control of precipitation kinetics by temperature and saturation state: *Am. J. Sci.*, 299, 257–288, 1999.

Boyd, C. E. Effects of ion-pairing on calculations of ionic activities of major ions in freshwater. *Hydrobiologia,* 80 (1), 91-93,1981.

Hanor, J. S. Reactive transport involving rock-buffered fluids of varying salinity, *Geochim. Cosmochim. Acta,* 65 (21)**,** 3721-3732, 2001.

Jones, G. D. *Numerical modeling of saline groundwater circulation in carbonate platforms*. Earth Sciences. UK, University of Bristol, 2000.

Logan, B. W. The MacLeod evaporite basin, Western Australia. *AAPG Mem.,* 44, 1987.

Lucia, F. J. Origin and petrophysics of dolostone pore space. In Braithwaite, C.J, Rizzi G., and Darke, G. (eds). *The geometry and petrogenesis of dolomite hydrocarbon reservoir*. Geol. Soc. Lond. Spec. Publ., 235, 141-155, 2004.

Lucia, F. J. Rock-fabric petrophysical classification of carbonate pore-space for reservoir characterization. *AAPG Bull.,* 79 (9)**,** 1275-1300, 1995.

Sanford, W. E., Whitaker, F. F., Smart, P. L. and Jones, G. D. Numerical analysis of seawater circulation in carbonate platforms: 1. Geothermal convection. *Am. J.. Sci.,* 298 (10), 801-828,1998.

Schmoker, J. W. and Halley, R. B. Carbonate porosity versus depth - A predictable relation for South Florida. *AAPG Bull.,* 66 (12)**,** 2561-2570, 1982.

Warren, J.K. *Evaporites: their Evolution and Economics.* Wiley Blackwell, 1999.

Xu, T., Sonnenthal, E., Spycher, N. and Pruess, K. *TOUGHREACT User's Guide: A Simulation Program for Non-isothermal Multiphase Reactive Geochemical Transport in Variably Saturated Geologic Media*, Report LBNL-55460, Lawrence Berkeley National Laboratory, Berkeley Calif., 2004.

Zhang, G., Spycher, N., Xu, T., Sonnenthal, E. & Steefel, C. *Reactive Geochemical Transport Modeling of Concentrated Aqueous Solutions: Supplement to TOUGHREACT User's Guide for the Pitzer Ion-Interaction Model*, Report LBNL-62718, 2006a.

Zhang, G., Spycher, N., Sonnenthal, E., Steefel, C. And Xu, T. Modeling Reactive Multiphase Flow and Transport of Concentrated Solutions Using A Pitzer Activity Approach with TOUGHREACT, *J. Nucl. Technol.*, 164(2), 180 – 195, 2006b.